AMAS Workshop on Image Analysis in Investigation of Concrete
SIAIC'02 – (pp.203–230) – Warsaw, October 21-23, 2002.

Classification of defects on the surface of black ceramics

L. CHMIELEWSKI, M. SKŁODOWSKI and W. CUDNY

Institute of Fundamental Technological Research
Świętokrzyska 21, 00-049 Warszawa, Poland
lchmiel@ippt.gov.pl
msklod@ippt.gov.pl
wcudny@ippt.gov.pl

Methods of visual detection and measurement of certain surface defects of black ceramics – magnets and ferrite cores – are presented. Difficulties such as dark colour of ferrite and variability of appearance of defects under different light conditions have been overcome. The monochromatic images of the product surface, taken under a highly specialised lighting system with a standard monochromatic digital camera, are processed with a hierarchical morphological irregularity detector, classified with a feature-based k nearest neighbours classifier, and postprocessed. The same methodology can be applied to other materials having similar appearance.

Key words: *quality inspection, surface defects, machine vision, pattern recognition, magnets, ferrite cores.*

1. Introduction

Ferrites are ceramic magnetic materials made of oxide powders. Ferrite cores are manufactured by compacting and sintering these powders, and by grinding some surfaces to required dimensions. Similar technology is applied in the production of other products made of black ceramics. The aim of the paper is a presentation of the methods of detection and measurement of certain surface irregularities which emerge in the manufacturing process of magnets and ferrite cores. The main difficulties encountered are: dark colour of ferrite, large variety of possible shapes and locations of defects, and variability of their appearance, even in typical light conditions [9].

The above circumstances have effectively prevented even the leading manufacturers of ferrites from automating the surface quality inspection of ferrite cores.

Manufacturers and buyers of ferrites distinguish tens of classes of defects. These comprise the defects of various surfaces, of shapes, and of the material. Standardisation institutions work on defining these defects, but their task is still far from finished. The defects emerge during the complex manufacturing process of a ferrite product, which comprises milling, moulding, pressing, sintering, grinding and finally, transporting.

In this research, *only some defects of the mating surfaces are considered.* The reason is twofold:

1. the ferrite manufacturers seem to agree that defect of the mating surfaces are of greatest importance and interest;
2. this group of defects seemed the most easily tractable, as the defects appear only on flat surfaces.

In setting acceptable dimensions of defects two types of criteria are usually taken into account. These are: proper operation of the product, and its appearance. In many cases the latter is more demanding, as in some locations quite large defects do not impair the functionality of ferrite core. The fact that some defects are acceptable gave rise to the use of a notion of *irregularity*, to avoid the negative connotation of the word *defect*. In this paper, however, the notion of *defect* will be used throughout.

The presented study concerns ferrite cores and magnets, but the same methodology can be used to investigate defects on flat surfaces in other similar materials, such as dark ceramics in general. Other surfaces, like white ceramics and painted surfaces, could also be treated in the similar way.

2. Overview of methods used

The monochromatic images of the irregularities of interest are acquired by the system consisting of a highly specialised lighting set-up, a standard digital camera, and a computer.

A hierarchical method for classification of a core with respect to surface irregularities has been applied. It consists of two main phases:

- **Detection phase.** Regions which might be a defect are detected. This phase is hierarchical in itself: the morphological pyramid technique has been used [10]. In detecting the defects of different sizes the structuring elements are kept the same, but the image is scaled down, to reduce the time of computations.
- **Classification phase.** Pixels of the regions selected in the detection phase are classified with a highly advanced version of the *k nearest neighbours* method [3, 4, 6]. The features used were selected from

a large number of possible deterministic, statistical and textural measures, with the use of numerous training samples.

The whole method is complemented by *postproccessing* the results of the classification phase.

Finally, the defects are measured, and the results are compared with quality standards to get the final classification of the product as belonging to a respective *quality class*. Quantitative nature of the measurements make them useful in analysis of the production process.

3. Types of defects

A pair of cores with their mating surfaces visible, and a plate magnet, can be seen in Fig. 1. Three types of irregularities are of main importance on surfaces: *chips*, *pull-outs* and *cracks*.

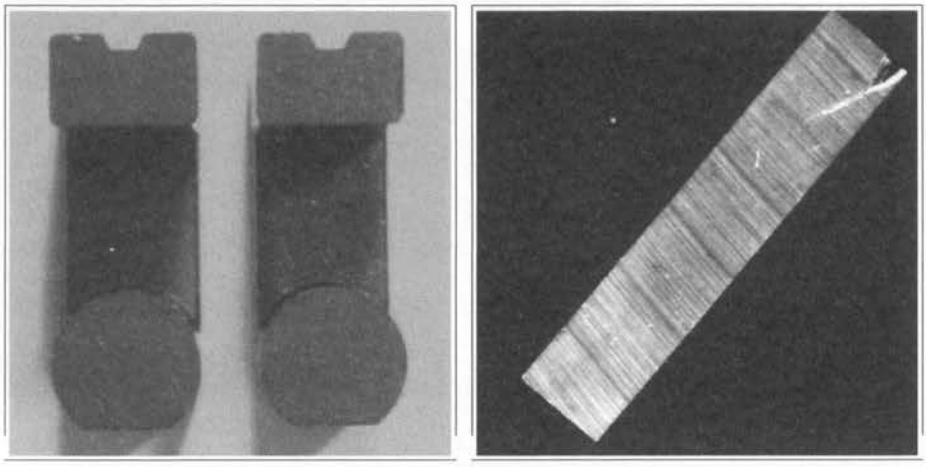

(a) (b)

FIGURE 1. The tested products. (a) A pair of ferrite cores with their mating surfaces visible. (b) A plate magnet with a visible defect.

A *chip* emerges where the material has been removed in the way of brittle cracking during grinding or as a result of another mechanical impact (Fig. 2a). A *pull-out* is a place from which the material has been taken away by a stamp during the pressing: some of the soft material has stuck to the stamp (Fig. 2b). A *crack* is the discontinuity of the material which appeared as the result of sintering the improperly pressed powder (Fig. 2c, d).

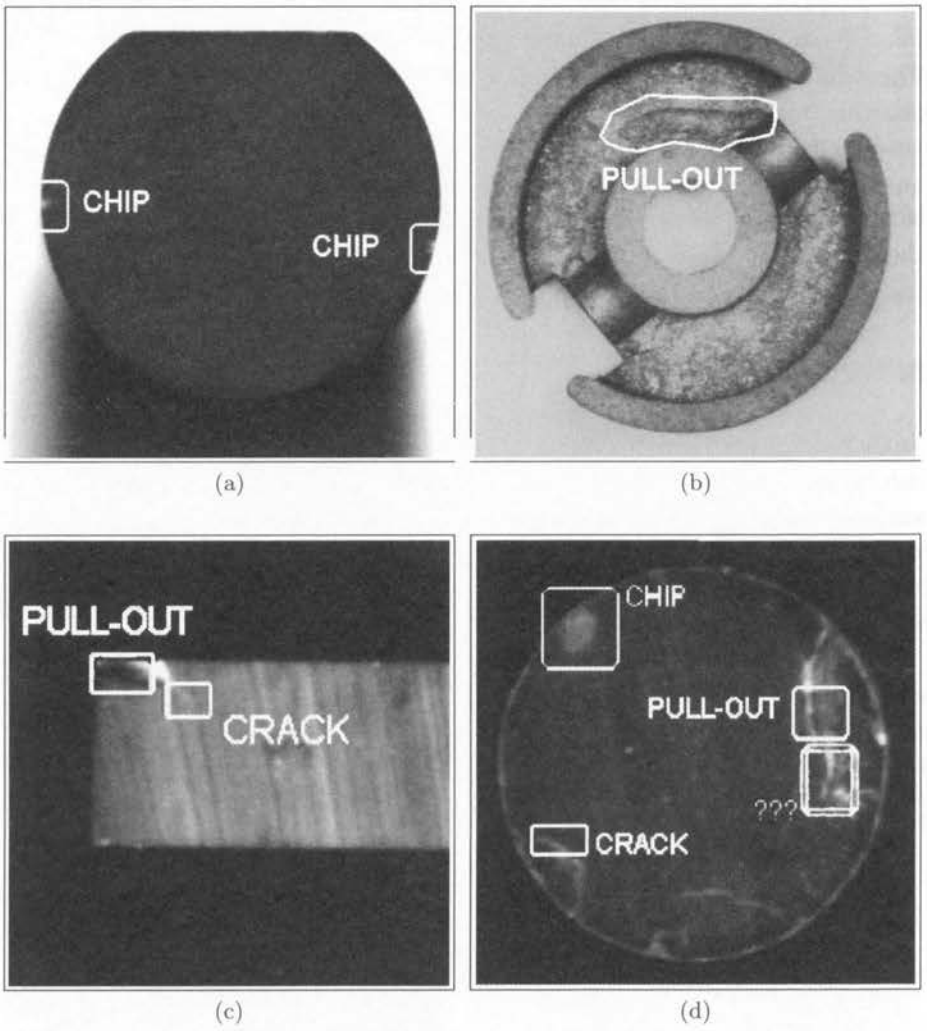

FIGURE 2. The most important surface defects. Chip – (a) and (d); pull-out – (b), (c) and (d); crack – (c) and (d). In (c) and (d) it can be seen how different types of defects can be difficult to classify univocally.

4. The problem of lighting

Due to the dark colour of the investigated objects, the proper lighting becomes vital. In the quality inspection of the considered objects made by a human, the inspecting person is able to move the tested object with respect to the light source and to the eye, so that the defects of the surface are best visible. The angle of light reflection can be then set in such a way that the

contrast of the irregular parts of the surface with respect to the normal parts becomes large. This tuning is done, to the large extent, in an intuitive way.

Such a process would be difficult to model in an automatic system. One of the possible, simplified approaches, would be to use a limited number of light sources, illuminating the surface from different direction, and use them for each investigated surface in sequence, seeking for the best effect. The data derived from multiple images of each surface should be merged to receive the combined result. Such an approach could be studied as the next step of investigations, but at present, mainly due to the processing time requirements, it has been decided to find out how much information can be extracted from a single view of the surface.

In designing the lighting system the following requirements have been taken into account:

1. maximum insensitivity to position and direction of the object in the field of view;
2. insensitivity to change of distance between the tested surface and the camera (within some range);
3. possibly large contrast of defects;
4. possibly large difference between irradiation of the tested surface and of other visible surfaces on the tested object and the base.

The first requirement stems from the considerations given above. The second one is necessary because the tested objects can differ in height to some extent.

After some experiments, a lighting similar to natural diffused light has been excluded. This was mainly because the requirements 3 and 4 were im-

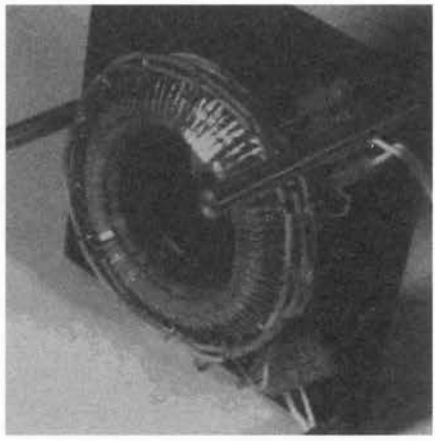

FIGURE 3. Double Layered LED Illuminator (DLEDI) – bottom view.

possible to satisfy with such a light. Six different circular lighting systems have been designed and manufactured or bought. From among them, the two tangential light systems have been selected as the best ones: the Double Layered LED Illuminator (DLEDI), Fig. 3, and the Variable Light Beam Illuminator (VLBI), Fig. 4 and 5. Both illuminators provide a very uniform irradiation of the tested surfaces (Fig. 6), while the VLBI better meets the requirements 3 and 4. The results presented in this work have been obtained with the VLBI.

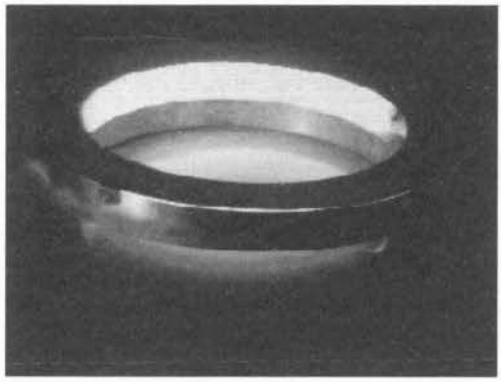

FIGURE 4. Variable Light Beam Illuminator (VLBI) – side view.

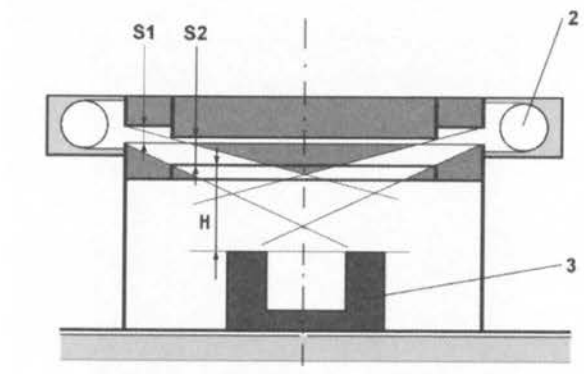

FIGURE 5. Variable Light Beam Illuminator (VLBI) – design. S1, S2 – movable diaphragms; 2 – toroidal fluorescent bulb; 3 – tested object; H – distance from the illuminator base to the object surface.

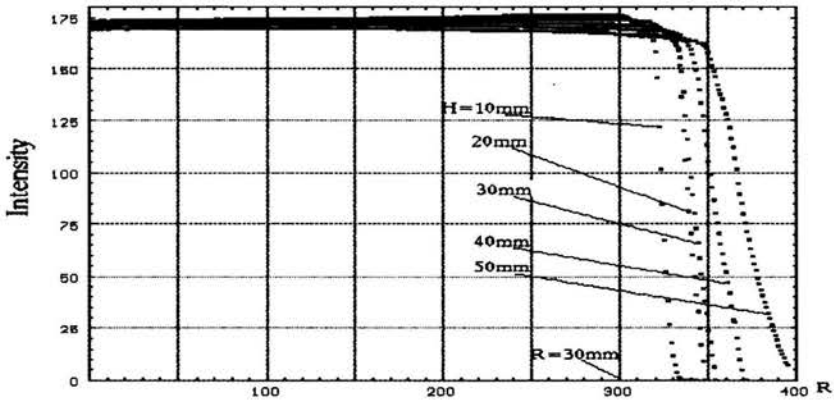

FIGURE 6. A very good uniform radial illumination distribution for the VLBI at various distances H from illuminator base to the object surface (see Fig. 5). Similarly for DLEDI.

5. The detection phase – finding the region of interest for classification

The classification of the regions of the object of interest is a relatively time-consuming operation. It is necessary to restrict the analysed part of the image to the regions which may actually contain a defect. This operation can be treated as finding the region of interest (ROI) for further processing. It consists of two stages. In the first, the region of the object is found. In the second, this region is analysed to find the subregions which have irregular brightness. The first phase will be described below in detail, while the second stage, which is a complex process in itself, has been described in another chapter of this book [12], and will be only briefly treated here.

5.1. Detecting the object without the model of the object

5.1.1. Contradictory actions of opening and closing. Under the non-directional, uniform and tangential lighting, used in the Project to lighten the surfaces of the tested objects, the objects cast deep shadows in their vicinity, while far from the objects there can be some reflections from the background. A good example of this phenomenon can be seen in Fig. 7a. The image seems to have very good contrast, so it seems that to find the silhouette of the object a simple thresholding should be sufficient. However, the thresholding fails, irrespective of the threshold – see Fig. 7b.

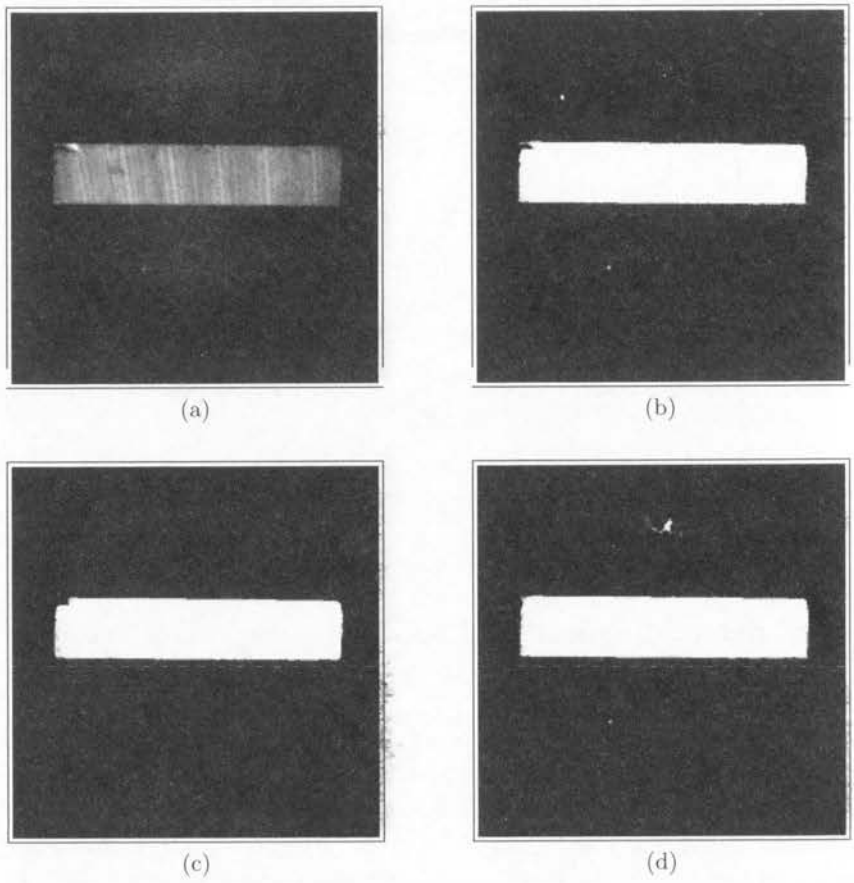

FIGURE 7. Contradictory actions of opening and closing. (a) An object surrounded by dark region and some brighter spots far from the boundary. (b) Image (a) thresholded: either parts of object left out or outer spots detected. (c) Image (b) opened – background cleared, object incomplete (structuring element: 11×11 round). (d) Image (b) – object gaps filled in, background spots enlarged.

An effective means for removing unnecessary small spots from the background of the image is the opening operation. The result of opening the image of Fig. 7b is shown in Fig. 7c. On the other hand, if an object has a defect at the boundary, as it is the case in Fig. 7a, it is necessary not only to detect the bright parts of the object, but also to fill in the dark parts missing after the thresholding. This can be easily done with the use of the closing operation – see the result in Fig. 7d.

In this way, a following contradiction appears. We seek to discern the object from the background. To clear the background of the thresholded

image, the opening is necessary. To fill in the gaps in the object, the closing is necessary. In fact, opening should be done in the background, and closing in the object. But it is just the object and the background that we are looking for.

5.1.2. Finding approximate background by scaling down. The method proposed to solve the above described contradiction is based on two assumptions:

1. the object is the largest bright blob in the image;
2. the bright spots outside the object are relatively far from its boundary.

Scaling the image down reduces the brightness of the small blobs, provided that it is not performed in the way of subsampling, but rather in the way of smoothing (averaging of brightness in the regions of the input image which become a single pixel in the output image). Such scaling makes small details disappear (also on the boundary of the object). Assume the scaling down eight times is performed (Fig. 8a), thresholding (b), and the following back-scaling by multiplication of rows and columns. The maximum error of location of the boundary at the output with respect to the input image is eight pixels. To avoid missing any of the original object pixels in the output, dilation with an element with half-width equal to eight pixels is necessary (round element is used to avoid direction-related phenomena; a sequence of dilations with smaller elements can be applied (Fig. 8c).

FIGURE 8. Finding the approximate background. (a) Image of Fig. 7a scaled down – brightness of background spots reduced. (b) Image (a) thresholded with the same threshold as in Fig. 7b. (c) Result: image (b) scaled back and dilated (original object overlaid only for comparison).

5.1.3. Final result. Having the approximate shape of the background, it is possible now to modify the mask of the object corrected by dilation, but still having erroneous pixels coming from the bright spots in the background, as seen in Fig. 7d, by setting to zero the brightness in the background just found. The result can be seen in Fig. 9a. Now, the source grey image of Fig. 7a can be modified by setting to zero the pixels which are zero in this bi-level image. The final result is shown in Fig. 9b.

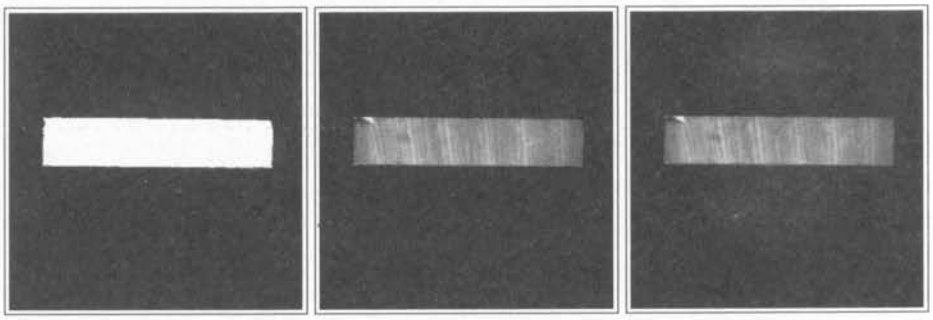

FIGURE 9. Solution of the problem of object finding. (a) Mask of the object: minimum of images of Fig. 7d and 8c (a 1-pixel error visible near the lower boundary of the object). (b) Modified input image of Fig. 7a – (nearly) all the background is set to zero. (c) Source image of Fig. 7a shown for comparison.

5.2. Finding the regions with irregular brightness

The defects in the ferrite cores manifest themselves as regions of irregular, or untypical, brightness. The detection of such regions can be very well described and solved in terms of the mathematical morphology. The applied methods have been described in detail in another chapter of this book: *Extraction of Surface Defects Using Morphological Pyramid and Watershed – Example of Ferrite Cores*, by Mariusz Nieniewski. Here let us show some examples of results of such detections shown in Fig. 10.

6. Feature-based classification of the detected regions

The pixels marked in the detection phase are treated as patterns for further classification. Each single pixel is a pattern. Its features are found as functions defined on its square neighbourhood, called *simple neighbourhood*. To have direction-invariant features, besides the simple one, a *rotated neighbourhood* is used. The edges of the rotated neighbourhood are placed

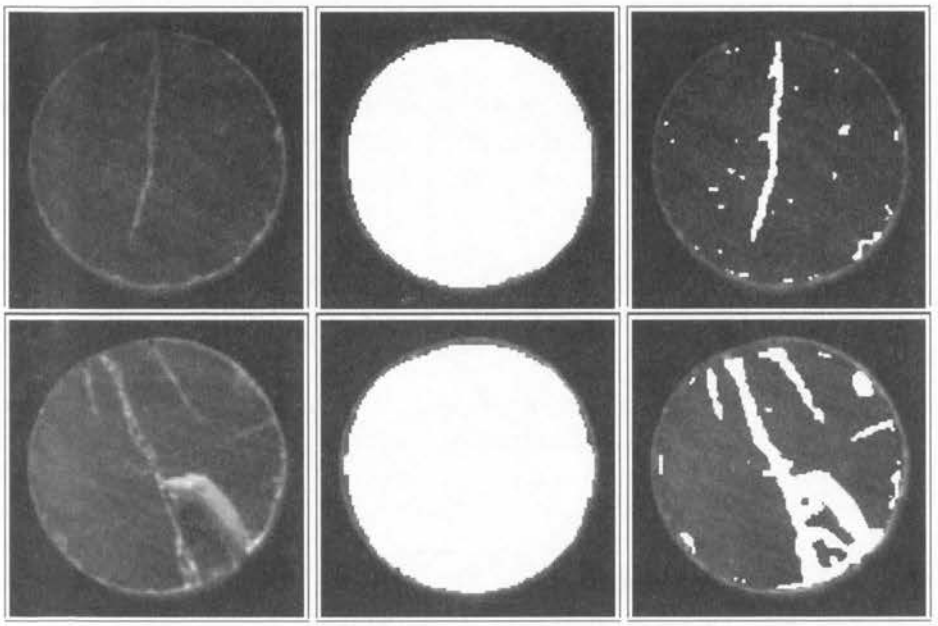

FIGURE 10. Detection of the region of interest (white) for defect classification – two examples (rows). (a) Source images. (b) Detected region of the object, as described in Section 5.1 (narrow stripe at the object edge deliberately postponed). (c) Regions with irregular brightness detected with the methods of mathematical morphology.

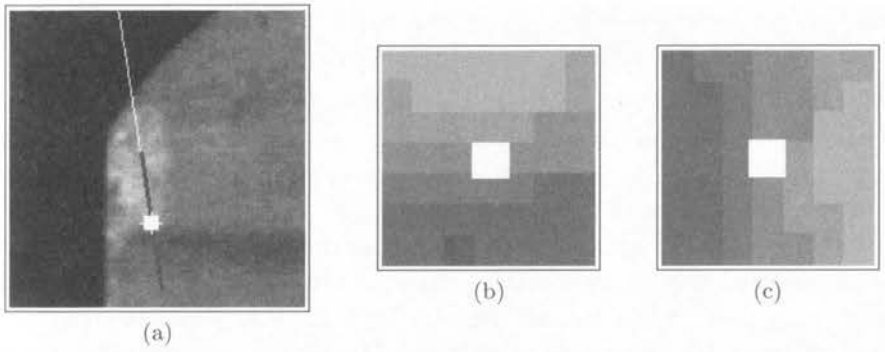

FIGURE 11. (a) Pixel with the normal to the dominating direction of texture marked. (b) Simple 7×7 neighbourhood of this pixel, used for direction calculation. (c) Rotated 7×7 neighbourhood.

along the dominating direction of texture, calculated locally in the simple neighbourhood, according to the spectral method proposed in [15]. The final equation for direction, derived there, necessitates only for the first-order partial derivatives of the image brightness function I, which are readily available in their numerical approximations. The equation is as follows:

$$\tan\left(2\theta - \frac{\pi}{2}\right) = \frac{\int\limits_{\Omega} 2\,\frac{\partial I}{\partial x}\frac{\partial I}{\partial y}\,dx\,dy}{\int\limits_{\Omega}\left[\left(\frac{\partial I}{\partial x}\right)^2 + \left(\frac{\partial I}{\partial y}\right)^2\right] dx\,dy}, \tag{6.1}$$

where Ω is the area of the simple neighbourhood and θ is the angle between the sought direction and the x axis. An example of a simple and a rotated neighbourhood is shown in Fig. 11.

Several groups of features have been tested. Those intrinsically rotation invariant were calculated from the simple neighbourhood only. The list of the considered features follows:

1. raw brightnesses in the simple neighbourhood;
2. raw brightnesses in the rotated neighbourhood;
3. statistical moments of brightnesses in the simple neighbourhood, of order 2 up to R;
4. same as 3, but in the rotated neighbourhood;
5. modulus of gradient in the simple neighbourhood;
6. textural features according to [8], described also in [13];
7. same as 6, but in the rotated neighbourhood;
8. textural features based on the concurrence relations, according to [14];
9. same as 8, but in the rotated neighbourhood;
10. section of brightness function along the line according to θ.

In the experiments, from 30 to 150 features were used at a time. Larger numbers would also be applicable in the recognition phase, but they would be too much time-consuming for the feature selection algorithms. From the experience gathered until now it follows that the feature set usually selected as optimum usually consists of 9 features of group 7 (all 9 measures of texture introduced in [8]) and features of group 10, usually first 21 features.

The group 10 needs an explanation. The *section of brightness function* has been designed to reflect long-distance brightness relations, with large number of features like in groups 1 and 2 avoided. A line section centred at the pixel of interest, according to the dominating texture direction (as marked with a broader line in Fig. 11a) is drawn in the picture. It passes

through other pixels which lie symmetrically around this central pixel. Let us index the central pixel with index 0, the pixels towards darker region of the image – with positive indexes, and towards the opposite direction – with negative indexes. Then the subsequent features are calculated as indicated in Table 1.

TABLE 1. Calculation of features from group 10 – section of brightness function (see text).

Feature	1	2	3	4	5	...
Value	$I(0)$	$\frac{I(1)}{I(0)}$	$-\frac{I(1)}{I(0)}$	$\frac{I(2)}{I(0)}$	$-\frac{I(2)}{I(0)}$	...

The selected features made it possible to get very satisfactory final results of recognition (see Sections 10 and 12).

7. K nearest neighbours classification

The well known classification method *of k nearest neighbours* (k-NN) has been used [1, 2]. The basic version of this method is the following (see Fig. 12). Assume that a set of patterns from each class is given. The sum of these sets is called the *training set*. To recognizee an unknown pattern it is necessary

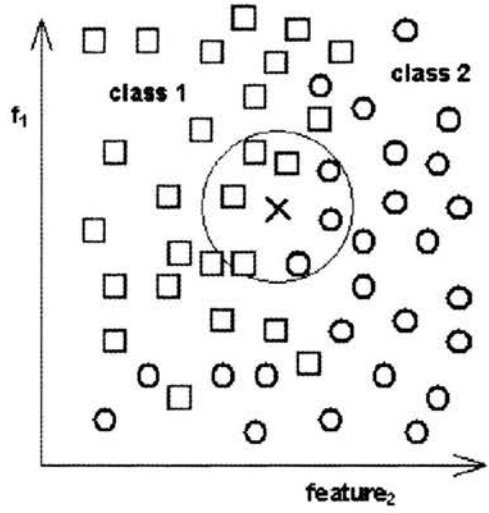

FIGURE 12. The basis of the k nearest neighbours classification – the case of $k = 7$. The unknown object (cross) is classified as belonging to the class 1 (squares), because among its 7 nearest neighbours the majority belongs to that class.

to find its k nearest neighbours in the feature space. The unknown pattern is assigned to the class to which the majority of these k neighbours belong.

The method is known for very quick training. Actually, no training is needed in a sense like for example in case of a neural network. Training a k-NN classifier is carrying out feature selection and choosing the value of k. This can be done effectively, even with simple strategies of search in the parameter space. A good criterion is minimum overall error or minimum of the maximum inter-class error. This criterion has been used in the present work. Errors can be precisely estimated on the whole available set of training patterns with the use of the *leave-one-out* method.

Here, a highly advanced version of the k-NN method has been used. It can be described by the following properties:

1. fuzzy [3];
2. parallel – there is a separate classifier for each pair of classes, and the classifiers vote;
3. with full selection of features and k - separately for each classifier;
4. hierarchical – a simple 1-NN version is used where classes do not overlap in the feature space [4];
5. with reduced set of reference patterns – sets of reference patterns for classes contain only those training patterns which influence the class boundaries in the feature space.

The properties 1, 2 and 3 improve the quality of classification. Property 3 gives some improvement in efficiency as a side-effect. Properties 4 and 5 have been introduced exclusively for efficiency. They make it possible to reach a desired point in the efficiency-quality trade-off. In the present work the requirement of classification quality has been promoted, and the reference patterns set has been reduced as much as possible, but without letting the recognition results change to worse for any initial training pattern. Intensive work on further speeding up the classification algorithm and improving its generalisation power is currently being carried out [5, 6, 7].

8. Training patterns

For training, the *ground truth* data have been provided by *manually* marking with colours the pixels which belong to classes in the training images, made of the training batch of cores. This difficult task has been possible to fulfil only with looking at the original core. Frequently a magnifying glass was helpful.

The colour codes shown in Fig. 13 and described in Table 2 have been used. Please note that *artificial, boundary classes* formed with pixels lying

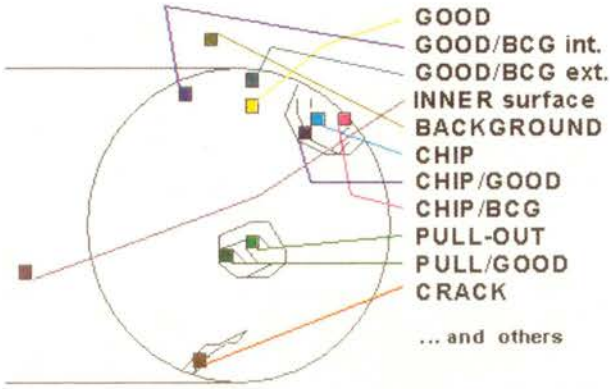

FIGURE 13. Locations and colour codes of classes and boundary classes of defects and correct surfaces used throughout the paper. Colour components specified in Table 2 (p. 219).

(a) (b) (c)

FIGURE 14. Postprocessing by spanning the convex hull. (a) Original image – a very large chip. (b) Classified. (c) Postprocessed. (Figure belongs to Section 9.1, p. 219).

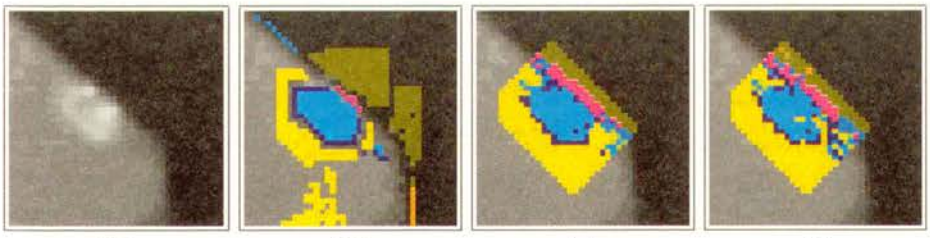

(a) (b) (c) (d)

FIGURE 15. Generalisation power in classification with and without the reduction of the training set. (a) Original. (b) Training data. (c) Classified without reduction. (d) Classified with reduction. (Figure belongs to Section 10, p. 221).

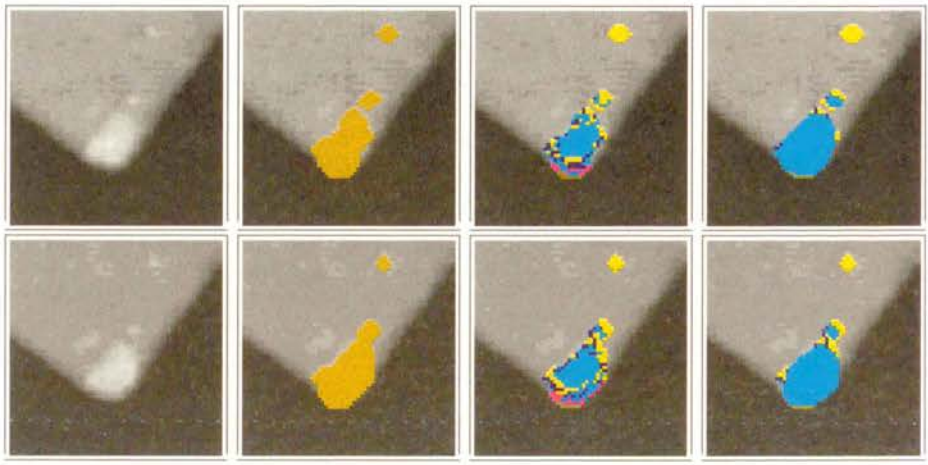

(a) (b) (c) (d)

FIGURE 16. Generalisation power of the classifier and invariance to small lighting changes. Upper row: light I; lower row: light II. (a) Originals. (b) Detected irregular regions. (c) Classified with reduction of reference set. (d) Postprocessed. Results for light I and II do not differ significantly. (Figure belongs to Section 10, p. 221).

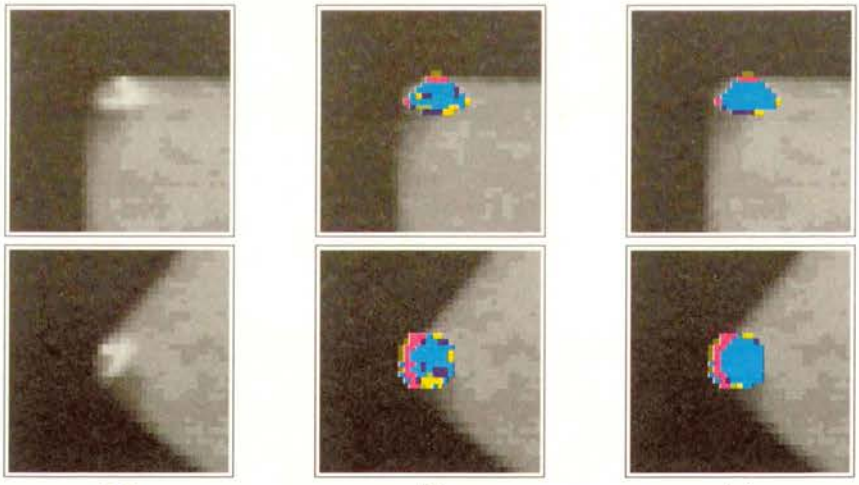

(a) (b) (c)

FIGURE 17. Generalisation power of the classifier and invariance under rotation and shift of the tested object. Upper row: object in position I; lower row: the same object in position II. (a) Originals. (b) Classified with reduction of reference set. (c) Postprocessed. Results for both positions do not differ significantly. (Figure belongs to Section 10, p. 221).

at the boundaries between physical classes have been introduced. This has led to better accuracy, as it has become possible to perform the choice of classifier parameters for more specific class pairs.

TABLE 2. Colour components of classes used in all the examples (range 0-255).

#	R	G	B	Class name
1	255	255	0	GOOD surface
2	128	128	0	BACKGROUND
3	0	255	255	bright CHIP
4	0	128	255	bright CHIP int. edge
5	150	150	255	bright CHIP ext. edge
6	0	192	192	dark CHIP
7	0	255	0	bright PULL-OUT
8	150	255	150	bright PULL-OUT edge
9	0	192	0	dark PULL-OUT
10	255	0	0	bright CRACK
11	255	64	28	bright CRACK edge
12	160	0	0	dark CRACK
13	0	128	128	ragged edge (series of small chips)
14	255	192	0	bright SPOT

In the initial experiments as much as 50,000 pixels have been used for training. Later, with the insertion of the boundary classes, usually less than 6,000 training pixels were used. Separate sets of training patterns were prepared for each type of object.

9. Postprocessing and decision making

9.1. Convex hull and merging

The vast majority of the irregularities are *convex*. On the other hand, the detector as well as the classifier tend to make errors inside larger defects. It is a straightforward idea to span a *convex hull* over the blobs which represent irregularities. The experiments indicate that indeed this improves the quality of classification results.

The merging is carried out as follows: all the sub-classes representing one class are merged together. Blobs formed in this way, which are closer to each other by less than 6 pixels, are merged (graphically linked to one another with a thin line). Further, a convex hull is spanned over each of the resulting blobs. An example of results for the class *chip* can be seen

in Fig. 14 (p. 217), where sub-classes of this class are merged (classes 3, 4, 5 and 6, see Fig. 13 in p. 217 and Table 2 in p. 219). This is an untypical, extraneously bad result of classification, presented to illustrate the potential of the proposed postprocessing method. Other, more realistic examples can be seen in Fig. 16 (p. 218) and 17 (page 17) which belong to Section 10.

9.2. Filtration by local weighted voting

After classification, pixels belonging to a specified class appear in groups (blobs) representing a physical irregularity. The pixels are classified separately, without taking into account the context (neighbouring pixels). The resulting maps of classes are irregular, and in each classified region there are pixels belonging to many classes. This phenomenon is strictly related to that even a human is usually not sure to which class a given small irregular region should be classified. For example, a region which can be classified as *chip*, may pass in a continuous way into a *pull-out*, and further may give an origin to a *crack* stemming from it on one end.

A process of local weighted voting has been used to implement, to some extent, the process of taking the context of a pixel into account. For a given pixel, all the pixels which belong to its 5×5 neighbourhood, centred on the considered pixel (including the pixel itself) vote for a class number. The votes are weighted with the weights shown in Table 3. Entries in this table have been calculated from the Gaussian function, with the standard deviation set to 3.

TABLE 3. Weights for voting used in postprocessing the classification results.

0.018	0.082	0.264	0.082	0.018
0.082	0.368	0.607	0.368	0.082
0.264	0.607	**1.000**	0.607	0.264
0.082	0.368	0.607	0.368	0.082
0.018	0.082	0.264	0.082	0.018

It can be questioned why the 5×5 neighbourhood was chosen and why the weights were set up in this and not in another way. The answer to both questions is the same: because the received results were then satisfactory. A smaller neighbourhood could also be used, with more passes of the process made in sequence, but this would be more time-consuming, and the result would be very similar. The Gaussian curve was used to make the weights decrease favourably as the distance between the central pixel and the voting pixel grows, down to (nearly) zero everywhere outside the mask.

Examples of results of the postprocessing can be seen in Fig. 18 in Section 10 and in the images in Section 12. Better homogeneity of the results make the segmentation of the results and the final decision much easier.

9.3. Final decision making

After the whole surface of the image, that is, each of its pixels, is classified as belonging to one of the classes, the image can be segmented into blobs with the standard segmentation methods. The blobs representing the good surface or the background are of no significance. The blobs representing the defects are counted and their areas are calculated. These data are compared with the thresholds specified for the given task. For example, the area (or length) of the largest blob of each class, total area (or length) of blobs of this class, and the number of defects of this class can be compared with the relevant admissible values, specified for the classes. This finally leads to the decision whether the given object, visible in the image, should be treated as good or bad, as shown in Table 4. The data on the defects found in the given batch of objects can be stored for further statistical analysis.

TABLE 4. Results of classification of an image from Fig. 23 (p. 227), first row. Measures: max – largest blob, total – sum of blobs, thr – respective threshold; units: mm^2 – for AREA classes, mm – for LENGTH classes.

Class	Blobs	Type	max/thr	total/thr	Quality
chip	12	AREA	0.11/0.50	0.57/1.00	GOOD
pull-out	24	AREA	0.89/0.50	1.76/1.00	**BAD!**
crack	19	LENGTH	3.46/1.00	11.76/2.00	**BAD!**
Total detected irregular area				6.18	
Final classification					**BAD!**

10. Visual estimation of the quality of classification

The results of training presented in the previous Section leave some place for classification errors. Therefore, the final estimation of the quality of classification obtained with the considered inspection system must be estimated visually. Below, a number of phenomena will be exemplified with images:

1. overall quality of classification (Fig. 15-18, pp. 217, 218 and 223);
2. small differences between the results obtained without and with the reduction of the reference patterns set, while the reduction gave about 14 times classification speed-up (Fig. 15, p. 217);

3. generalisation power of the classifier: correct results for pixels not used for training (Figs. 16 and 17, p. 218, and especially Fig. 18, p. 223);
4. invariance of results to small lighting changes (besides that light stability is under control) (Fig. 16, p. 218);
5. invariance of results to rotation and shift (Fig. 17, p. 218, also Fig. 24, p. 228, belonging to Section 12);
6. limits of the method are reached if it is expected that the classifier will perform the task which, in given conditions, is too difficult even for a human (Fig. 19, p. 224).

In all the images, the colours used to denote the classes are those defined in Fig. 13 (p. 217) and in Table 2 (p. 219).

Results of Fig. 18 (p. 223) require some additional explanation. This figure shows the generalisation power of the classifier and the quality of postprocessing. This result was received with the limited set of 2479 training patterns, all of them indicated in just four images, shown in the left column. After training, the classification system was able to classify the whole irregular regions, detected with the methods of the mathematical morphology, as indicated in Section 5.2, with the satisfactory quality. The postprocessing with the local weighted voting made the results ready for use. This example shows that the methods proposed here can lead to usable results with the reasonably small effort sacrificed to the training.

In Fig. 19 the problem of discriminating the cracks from the grooves which resulted form coarse grinding of the surface of the ferrite core is presented. This task was accomplished, as described in [11], but it seems that the limits of the method have been reached. The views of the cracks and the grooves are very similar in the images. Only using the global information would make it possible to discern them with great certainty, while the methods described here use only local and middle-range information. In the training, 4553 pixels were used. In the object shown in Fig. 19, in which the object occupied about 55600 pixels, the detector found about 6600 pixels as irregular, and the classifier assigned about 1900 of them to the class crack, and the remaining ones to groove. From these 1900 pixels, about 600 were the false positive errors. The false negatives were very few in this example. The actual classification error rate was then about 9% (600/6600), while the estimate of this error found during the training with the leave-one-out method was 1.4%. This difference is the main reason why we consider this case as the example of the limits of the method.

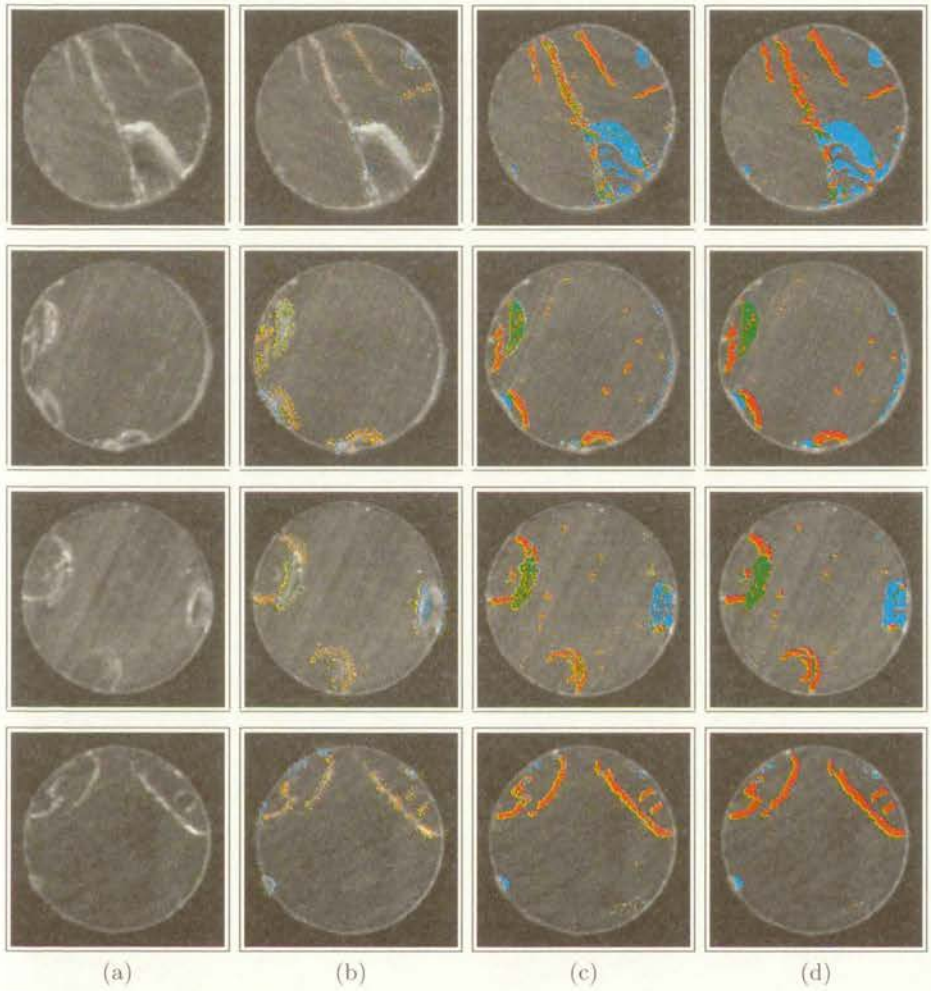

FIGURE 18. Generalisation power of the classifier. From top to bottom: four training images used in the experiment. (a) Source images. (b) All 2479 training patterns used to train the classifier, marked with colours. (c) Results of classification of the irregular regions. (d) The same results after postprocessing with the local weighted voting.

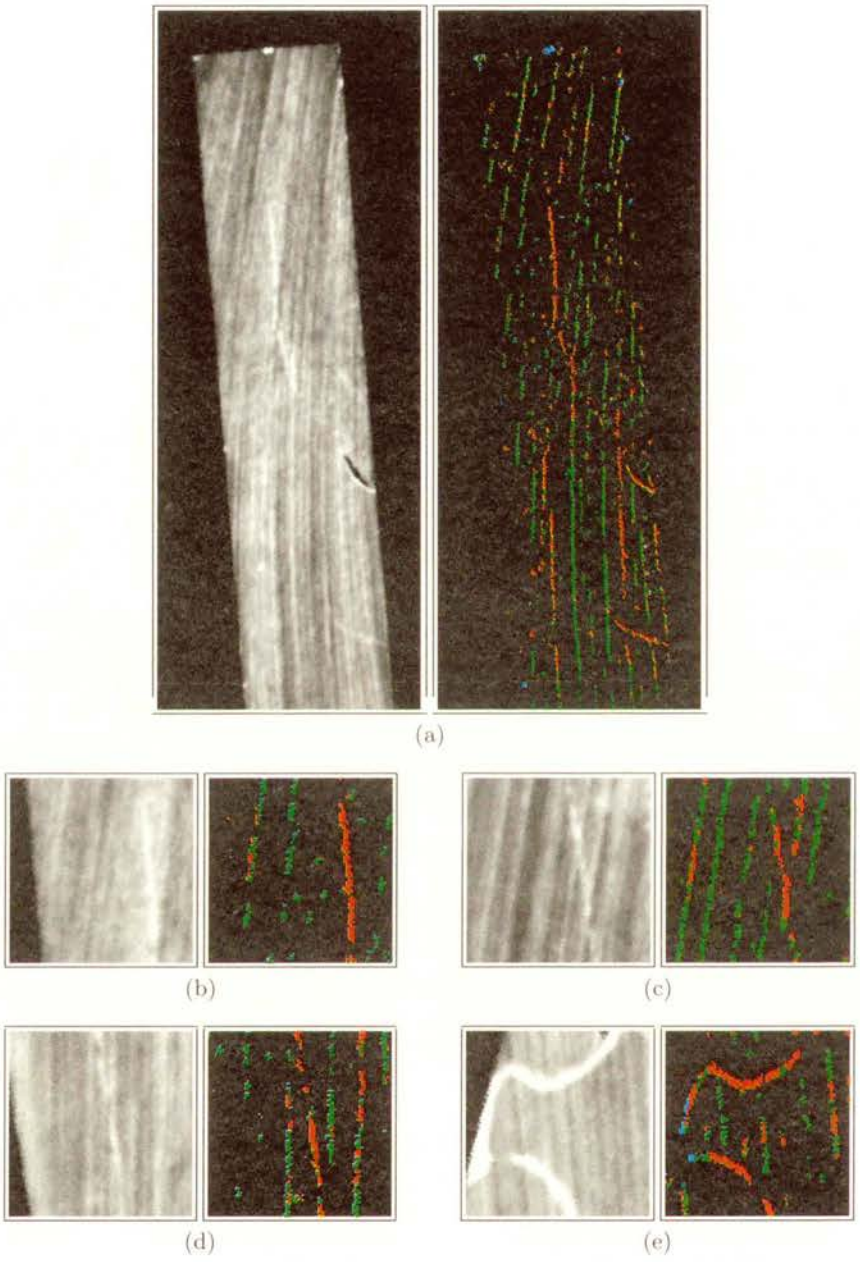

FIGURE 19. Example of the limits of the method: classification of the irregular regions into two classes: grooves from grinding (green) and cracks (red). Small chips (blue) also visible. (a) Source and classification result of the whole image. (b)-(e) details of this and other images.

11. Technical data and performance

The resolution of the majority of the analysed images was 500×500 pixels, which gives the spatial resolution of about 0.05×0.05 mm.

The classification errors were typically: overall 2.5% to 4%, inter-class up to 10% (in the case of boundary classes), typically less than 4% (see [7] or [5] for more details).

The repeatability of the results in relation to the area were as follows. In the detection phase, not worse than 2-5%. In the classification phase, not worse than 10-20%, depending on how fast a classifier was used.

The time of classification of 1000 pixels was about 1.2 s (PC, Pentium 1000 MHz; software – GNU C). In a typical 512×512 image, about 800 pixels are selected in the detection phase for classification, which would lead to the classification time of 1 s per image. The detection phase performed purely by software was about 2 s. For this phase the general-purpose morphological hardware can be used, which would lead to negligible, millisecond processing times.

The final segmentation and decision making time is negligibly small.

12. Examples of results

In this Section the examples of defect detection and classification in various ferrite products are presented. The images shown in Figs. 20-24, presented on pp. 225-228, do not require further explanations.

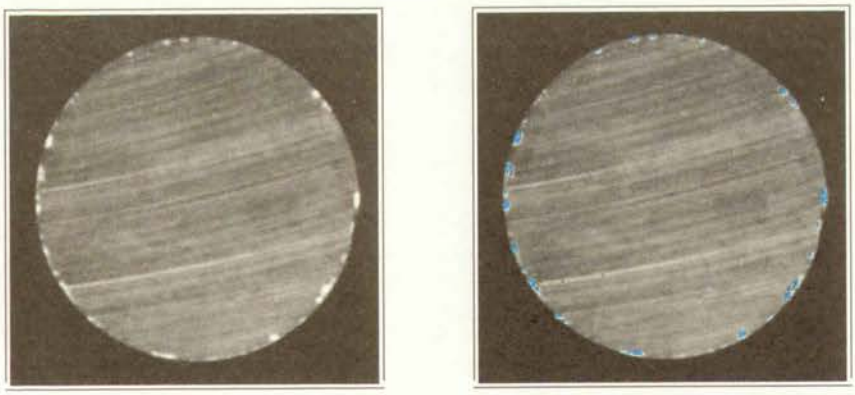

(a) (b)

FIGURE 20. Cylindrical magnets I, diameter 37.5 mm. Magnification: 0.121 mm/pix. 681 training patterns, 8 classes, 44 features. (a) Source image. (b) Postprocessed classification result.

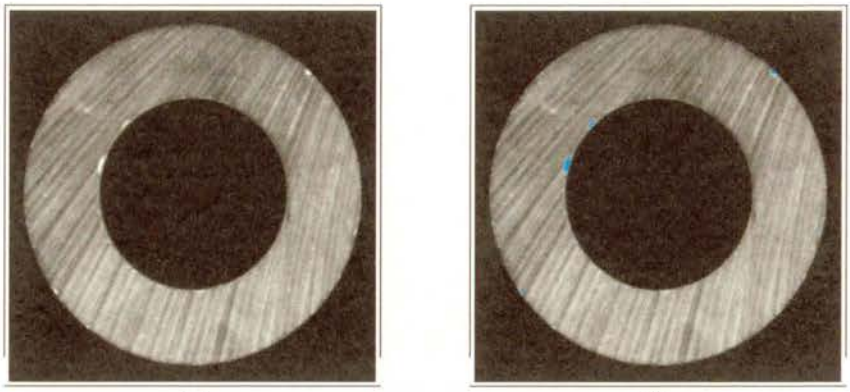

(a) (b)

FIGURE 21. Loudspeaker magnets I, diameter 50 mm. Magnification: 0.129 mm/pix. 1723 training patterns, 11 classes, 44 features. (a) Source image. (b) Postprocessed classification result.

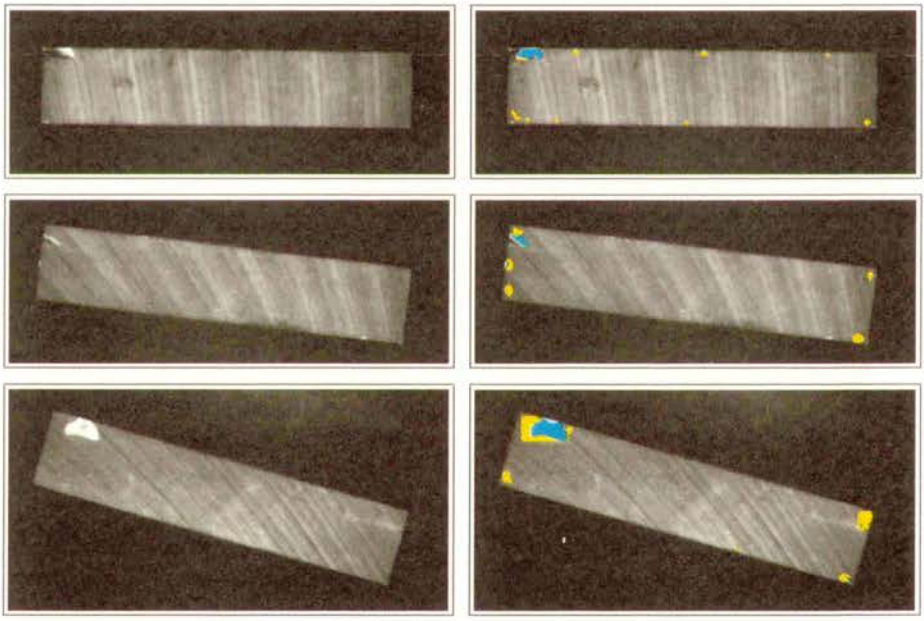

(a) (b)

FIGURE 22. Plate magnets, dimensions 60×12 mm. Magnification: 0.15 mm/pix. 2257 training patterns, 10 classes, 44 features. Object occupies approx. 400×80 pixels. From top to bottom: three examples. (a) Source images. (b) Postprocessed classification result.

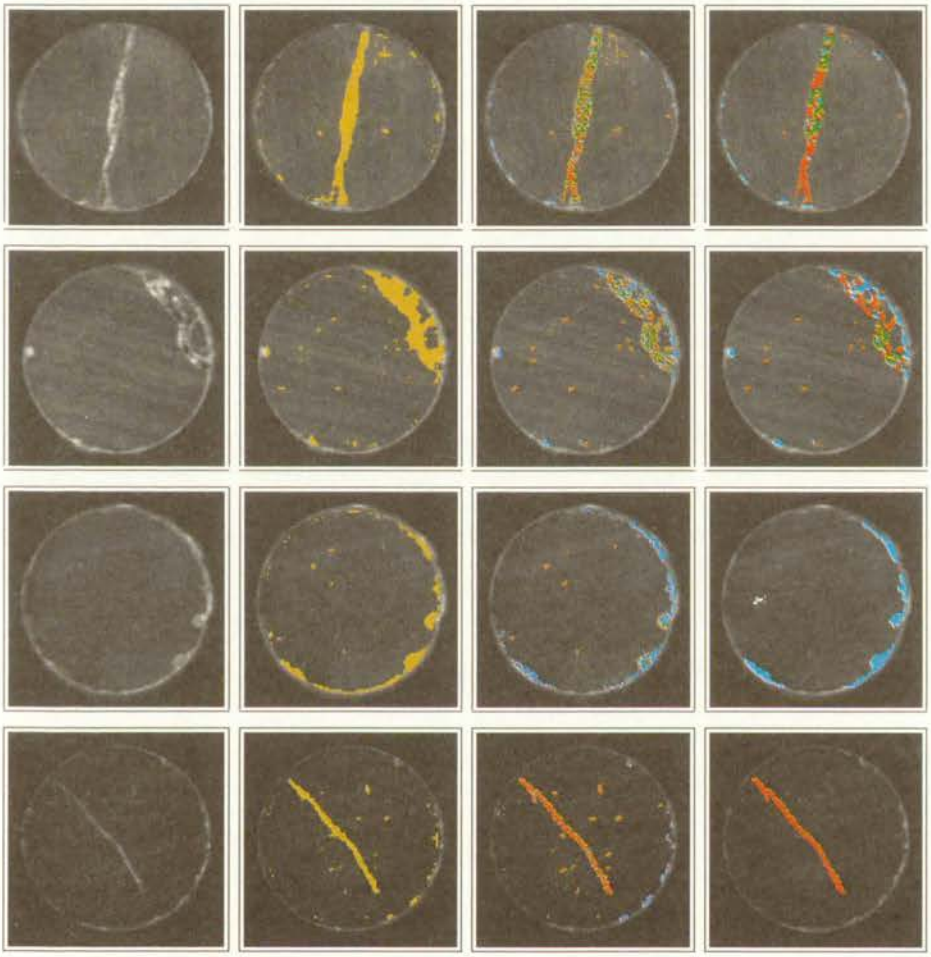

FIGURE 23. Cylindrical magnets II, diameter 10 mm. Magnification: 0.057 mm/pixel. 4279 training patterns, 14 classes, 64 features. From top to bottom: four examples. (a) Source images. (b) Detected irregular regions. (c) Raw classification results. (d) Postprocessed classification results.

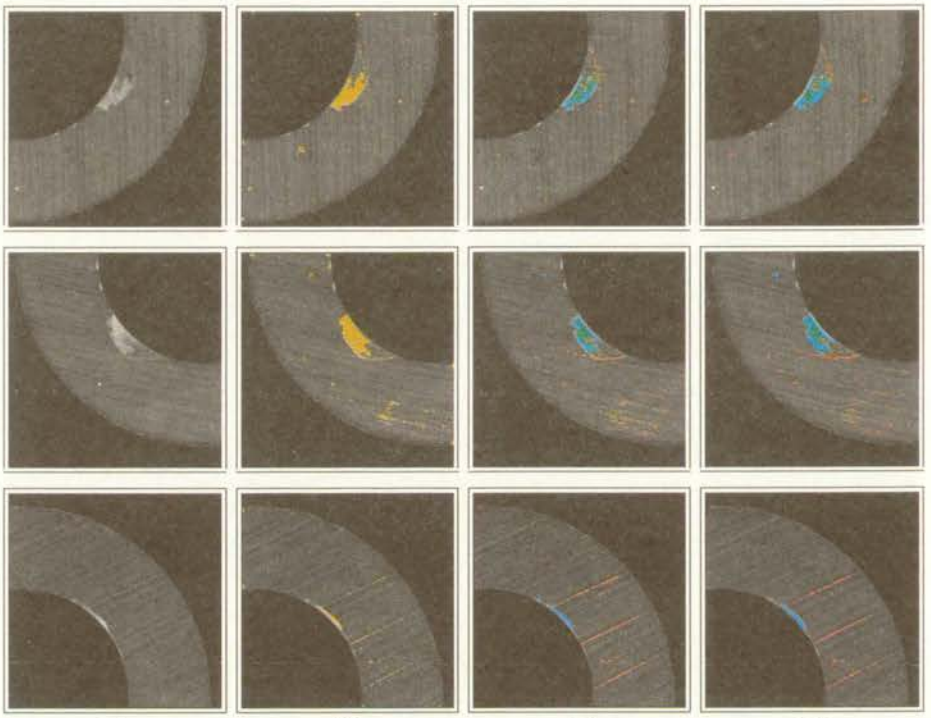

FIGURE 24. Loudspeaker magnets II, external diameter 50 mm. Same magnification and training as for cylindrical magnets of Fig. 20. From top to bottom: three examples. (a) Source images. (b) Detected irregular regions. (c) Raw classification results. (d) Postprocessed classification results. Note the problems with the grooves from grinding which seem as the cracks to the system. Upper and middle row show the different images of the same defect.

13. Conclusion

A hierarchical computerised optical inspection system for detection and classification of defects on flat surfaces of black ceramic products has been designed and implemented. The defects, which in the case of ferrite cores and magnets are called *irregularities*, belong to more than four different classes. Special attention has been paid to overcoming the difficulties related to dark colour of the tested objects and to attaining the invariance of the inspection process to such noncontrollable factors like scale of the defects and location of the object. Therefore, the applied image processing methods are local in general, in that the pixels of the image of the tested object are analysed in small

groups. Further postprocessing leads to finding the global characteristics of the product, like the size and number of defects of a specified type.

The system has been found to work properly in a series of tests. Some of the tests indicated where the limits of application of the presented system could be encountered. The performance of the system is sufficient for an application in the practical settings. The processing speed is acceptable in the laboratory environment, and for an industrial application, adding a standard mathematical morphology hardware processor would be enough.

The proposed methodology has been designed for the black ceramics, like magnets and ferrite cores. However, it has no intrinsic limitations against its application to detection of defects on flat surfaces also on the products other than those directly treated in this study, like, for example, painted surfaces, glass, or concrete.

Acknowledgement

This research was partially supported by the European Commission within the following projects: COPERNICUS grant *CRAck and SHape defect detection in ferrite cores (CRASH)* no. COP-94 00717 (1995-96) and INCO-COPERNICUS grant *Standard compliant QUAlity control System for High-level ceramic material manufacturing (SQUASH)* no. ERBIC 15CT 96 0742 (1997-98). In the case of both projects, the end-user was POLFER Magnetic Materials Co.Ltd. (Zakład Rdzeni Magnetycznych POLFER Sp. z o.o.), Warsaw.

References

1. J.C. BEZDEK, S.K. CHUAN, and D. LEEP, Generalized k-NN rules, *Fuzzy Sets and Systems*, Vol.18, pp.237-256, 1986.

2. B.V. DASARATHY, Nearest Neighbor (NN) norms: NN pattern classification techniques, *IEEE Computer Society Press*, 1995.

3. A. JÓŹWIK, A learning scheme for a fuzzy k-NN rule, *Pattern Recognition Letters*, Vol.1, pp.287-289, 1983.

4. A. JÓŹWIK, L. CHMIELEWSKI, W. CUDNY, and M. SKŁODOWSKI, A 1-NN preclassifier for fuzzy k-NN rule, in: *Proc. 13th Int. Conf. Pattern Recognition (ICPR'96), Wien, Austria, Aug. 25-29, 1996*, Vol.IV, pp.D-234–D-238, IAPR, Technical Univ. Vienna, 1996.

5. A. JÓŹWIK, L. CHMIELEWSKI, M. SKŁODOWSKI, and W. CUDNY, A parallel net of (1-NN, k-NN) classifiers for optical inspection of surface defects in ferrites, *Machine Graphics & Vision*, Vol.7, No.1-2, pp.99-112, 1998.

6. A. JÓŹWIK, L. CHMIELEWSKI, M. SKŁODOWSKI, and W. CUDNY, Class overlap rate as a design criterion for parallel Nearest Neighbour classifier, in: M. Kurzyński, E. Puchała, and M. Woźniak (Eds.), *Proc. 1st Polish Conference on Computer Pattern Recognition Systems KOSYR'99, Trzebieszowice, Poland, May 24-27, 1999*, pp.109-115, Wrocław University of Technology, 1999.

7. A. JÓŹWIK, L. CHMIELEWSKI, M. SKŁODOWSKI, and W. CUDNY, A proposition of the new feature space and its use to construction of a fast minimum distance classifier, in: M. Kurzyński, E. Puchała, and M. Woźniak (Eds.), *Proc. 2nd Polish Conference on Computer Pattern Recognition Systems KOSYR 2001, Miłków, Poland, May 28-31, 2001*, pp.381-386 Wrocław University of Technology, 2001.

8. K.I. LAWS, Textured image segmentation, USCIPI Report 940, Univ. of Southern California, Image Processing Institute, Jan. 1980.

9. M. MARI, C. DAMBRA, D. CHETVERIKOV, J. VERESTOY, A. JÓŹWIK, M. NIENIEWSKI, M. SKŁODOWSKI, , L. CHMIELEWSKI, W. CUDNY, and M. LUGG, The CRASH Project: Defect detection and classification in ferrite cores, in: A. Del Bimbo (Ed.), *Proc. 9th Int. Conf. Image Analysis and Processing. Number 1310 in Lecture Notes in Computer Science, Florence, Italy, Sept. 17-19, 1997*, Vol.II, pp.781-787, Springer Verlag, Berlin 1997.

10. M. NIENIEWSKI, Morphological method of detection of defects on the surface of ferrite cores. in: *Proc. 10th Scandinavian Conf. Image Analysis SCIA'97*, pp.323-330, Lappeenranta, Finland, June 9-11, 1997.

11. M. NIENIEWSKI, L. CHMIELEWSKI, A. JÓŹWIK, and M. SKŁODOWSKI, Morphological detection and feature-based classification of cracked regions in ferrites, *Machine Graphics & Vision*, Vol.8, No.4, pp.699-712, 1999.

12. M. NIENIEWSKI, *Extraction of surface defects using morphological pyramid and watershed: example of ferrite cores*, this volume: pp.175-201.

13. W.K. PRATT, *Digital Image Processing*, John Wiley, New York 1991.

14. C-M. WU and Y-C. CHEN, Statistical feature matrix for texture analysis, *Computer Vision, Graphics, and Image Processing: Graphical Models and Image Processing*, Vol.54, No.5 pp.407-419, 1992.

15. G.Z. YANG, P. BURGER, D.N. FIRMIN, and S.R. UNDERWOOD, Structure adaptive anisotropic filtering for magnetic resonance image enhancement, in: V. Hlaváč and R. Šára (Eds.), *Proc. 6th Int. Conf. Computer Analysis of Images and Patterns CAIP'95, Prague, Czech Republic, Sept. 6-8, 1995, LNCS*, Vol.970, pp.384-391, Springer Verlag, 1995.